Evidence of off-target probe binding in the 10x Genomics Xenium v1 Human Breast Gene Expression Panel compromises accuracy of spatial transcriptomic profiling

Caleb Hallinan[1,2], Hyun Joo Ji[1,3], Steven L Salzberg[1,2,3,4], Jean Fan[1,2,3]

[1]Center for Computational Biology, Whiting School of Engineering, Johns Hopkins University, Baltimore, MD 21211, USA

[2]Department of Biomedical Engineering, Johns Hopkins University, Baltimore, MD 21218, USA

[3]Department of Computer Science, Johns Hopkins University, Baltimore, MD 21218, USA

[4]Department of Biostatistics, Johns Hopkins University, Baltimore, MD

Correspondence should be addressed to:

Jean Fan (jeanfan@jhu.edu)

Abstract

The accuracy of spatial gene expression profiles generated by probe-based *in situ* spatially-resolved transcriptomic technologies depends on the specificity with which probes bind to their intended target gene. Off-target binding, defined as a probe binding to something other than the target gene, can distort a gene's true expression profile, making probe specificity essential for reliable transcriptomics. Here, we investigate off-target binding in the 10x Genomics Xenium v1 Human Breast Gene Expression Panel. We developed a software tool, Off-target Probe Tracker (OPT), to identify putative off-target binding via alignment of probe sequences and found at least 21 out of the 280 genes in the panel impacted by off-target binding to protein-coding genes. To substantiate our predictions, we leveraged a previously published Xenium breast cancer dataset generated using this gene panel and compared results to orthogonal spatial and single-cell transcriptomic profiles from Visium CytAssist and 3' single-cell RNA-seq derived from the same tumor block. Our findings indicate that for some genes, the expression patterns detected by Xenium demonstrably reflect the aggregate expression of the target and predicted off-target genes based on Visium and single-cell RNA-seq rather than the target gene alone. Overall, this work enhances the biological interpretability of spatial transcriptomics data and improves reproducibility in spatial transcriptomics research.

Introduction

Recent advances in high-throughput spatially-resolved transcriptomic profiling technologies have enabled the investigation of gene expression with high spatial resolution within tissues. One such commercially available spatial transcriptomics platform is Xenium from 10x Genomics, a publicly traded company with a market capitalization exceeding $1 billion as of March 2025 (Yahoo Finance 2025). Xenium achieves spatial gene expression profiling at single-cell resolution for targeted genes using a probe-based *in situ* detection approach. 10x Genomics currently offers targeted gene panels with pre-designed probe sets, including their 280-gene Xenium v1 Human Breast Gene Expression Panel. As of December 2024, over 16,000 Xenium consumable reactions have been sold, with each tissue slide profiled costing approximately $5,000, underscoring the platform's widespread use and high commercial value (10x Genomics).

Briefly, Xenium uses padlock probes that include sequences complementary to the RNA of target genes. Once a padlock probe binds to its target, it is ligated and subsequently amplified via rolling circle amplification (RCA). Fluorescently labeled decoder probes then hybridize to the amplified RCA product, enabling the simultaneous detection and decoding of the optical signature, or codeword, specific to each gene in the panel through successive rounds of fluorescence imaging. When combined with cell-segmentation, this approach allows for spatially-resolved single-cell quantification of gene expression.

53 The accuracy of these gene expression measurements thus relies on the specificity of the probes
54 to bind to their intended target gene. We define off-target binding as when a probe binds to
55 something other than the RNA sequence intended to correspond to the target gene (Figure 1).
56 We note once ligation and RCA occur, the resulting fluorescent signal cannot be distinguished
57 between on-target and off-target binding. As such, off-target binding can distort the
58 quantification of the intended target gene's expression, as the observed expression would
59 represent a combination of the target as well as off-target expression.
60

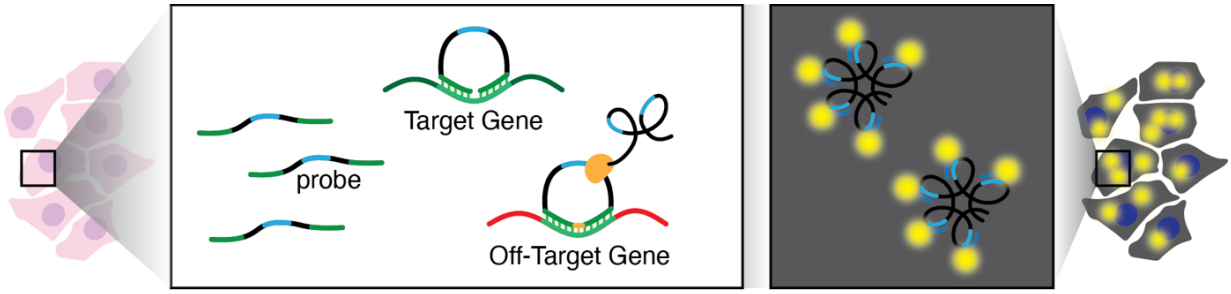

61

62 **Figure 1. Schematic of potential off-target binding in 10x Xenium.** In this illustration, the arms
63 of the padlock probes were designed to bind an RNA sequence intended to correspond to a target
64 gene (green). However, these probes exhibit off-target binding and bind to an RNA sequence in
65 a different off-target gene (red). The probe is circularized and subsequently amplified via rolling
66 circle amplification (RCA). Hybridization of fluorescent probes to the RCA product enables the
67 generation a fluorescent signal that is used to quantify RNA expression within cells.
68

69 To predict for such potential off-target binding, we developed Off-target Probe Tracker (OPT), a
70 software tool that aligns probe sequences to an annotated transcriptome with the option to
71 allow for mismatches that may still permit probe binding. Using OPT, we identify putative off-

target probe binding to protein-coding genes affecting at least 21 out of 280 genes in the 10x Genomics Xenium v1 Human Breast Gene Expression Panel, compromising the accuracy of their spatial transcriptomic profiles. We substantiate our predictions using data from orthogonal spatial and single-cell gene expression profiling technologies. By facilitating a more rigorous evaluation of probe sequence specificity, tools like OPT can aid in future probe design decisions to help ensure that probes are optimized to minimize off-target binding based on current transcriptome annotations.

Results

OPT predicts potential off-target probe binding

To identify potential off-target binding impacting the 10x Genomics Xenium v1 Human Breast Gene Expression Panel, we first downloaded the FASTA file containing the probe sequences from the 10x Genomics Website (Methods, Supplementary Data). This file includes 4,809 probe sequences that are 40bp in length and designed to target 280 genes, averaging 17 probe sequences per gene (ranging from 2 to 50 probe sequences per gene).

We developed a software tool called OPT (Methods) that uses nucmer (Marçais et al. 2018) to predict off-target binding by aligning probe sequences to a reference transcriptome, which comprises a curated collection of transcript isoforms for all genes in a species. OPT features

adjustable parameters for binding strictness (e.g., number of mismatches) and generates a summary file that details all targeted genes along with their potential off-targets based on the sequence alignments. 10x Genomics designed its probe sequences using the GENCODE “basic” annotation (Mudge et al. 2025), so initially we also used the latest GENCODE “basic” annotation (v47) to predict off-target binding for these probes.

We first sought to predict if a probe has off-target binding based on perfect sequence homology (i.e., if it aligns with 100% identity) with any annotated transcripts other than those that belong to the intended target gene. Of the 4,809 probe sequences in this gene panel, using GENCODE v47, OPT identified 180 probe sequences across 45 genes as having off-target binding based on perfect sequence homology (Table 1). Among the 45 genes with predicted off-target binding, the number of affected probe sequences per gene ranged from 1 to 14. Overall, these off-target probes matched 90 other genes, including 34 protein-coding genes, 34 pseudogenes, 12 long non-coding RNA, 9 transcripts labeled as nonsense-mediated decay, and one microRNA gene.

Target gene	Number of probes	Predicted binding genes	Number of probes aligned	Gene types - GENCODE (v47)
ADGRE5	19	ADGRE5,ADGRE2	19,1	PC,PC
ADH1B	23	ADH1B,ADH1A,ADH1C	22,3,3	PC,PC,PC
AKR1C1	21	AKR1C1,AKR1C5P,AKR1C2,AKR1C3, AKR1C4	21,1,1,1,1	PC,PC,PC,PC,PG
AKR1C3	17	AKR1C3,AKR1C1,AKR1C2,AKR1C4	17,1,1,2	PC,PC,PC,PC
APOBEC3A	10	APOBEC3A,APOBEC3B	8,4	PC,PC
APOBEC3B	14	APOBEC3B,APOBEC3D,ENSG00000284554, APOBEC3F,APOBEC3A	14,2,2,2,2	PC,PC,PC,PC,PC
AQP1	19	AQP1,ENSG00000250424	19,4	PC,PC
C15orf48	6	C15orf48,MIR147B	6,1	PC,miRNA
C1QA	4	C1QA,ENSG00000289692	4,2	PC,PC
CD68	7	CD68,ENSG00000264772	7,6	PC,lncRNA
CD79B	5	CD79B,ENSG00000285947	5,3	PC,PC
CEACAM6	13	CEACAM6,ENSG00000267881,CEACAM3	13,1,1	PC,PC,PC
CLECL1; CLECL1P	7	ENSG00000293488,CLECL1P	3,3	lncRNA,PG
DPT	18	DPT,LINC00970	18,13	PC,lncRNA
EPCAM	15	EPCAM,ENSG00000225356	15,1	PC,PG
FCGR3A	20	FCGR3A,FCGR3B,ENSG00000289768	20,3,3	PC,PC,PC
HMGA1	7	HMGA1,HMGA1P3,HMGA1P1,HMGA1P2	7,1,1,1	PC,PG,PG,PG
IL2RG	14	IL2RG,ENSG00000285171	14,11	PC,NMD
KLRC1	15	KLRC1,KLRC2,KLRC4-KLRK1,KLRC3, KLRC4,ENSG00000255641	15,3,1,1,1, 1	PC,PC,PC,PC,NMD,PC
KRT14	6	KRT14,KRT16P6,ENSG00000290977	6,1,1	PC,lncRNA,PG
KRT6B	15	KRT6B,KRT6C,KRT75,KRT6A	15,4,1,1	PC,PC,PC,PC
KRT8	18	KRT8,KRT8P11,KRT8P2,KRT8P3,KRT8P36, KRT8P45,KRT8P33,KRT8P37, ENSG00000304440,CDK5R2-AS1,KRT8P30, KRT8P17, KRT8P22,KRT8P32,KRT8P42	18,1,2,3,1, 2, 2,1,1,1,1,1, 1,1,1	PC,lncRNA,lncRNA,PG,PG,PG, PG,PG,PG,PG,PG,PG,PG,PG,PG
LDHB	18	LDHB,ENSG00000285854,LDHBP2	18,12,1	PC,NMD,PG
LILRA4	16	LILRA4,ENSG00000275210	16,3	PC,lncRNA
MYLK	35	MYLK,MYLKP1	35,1	PC,PG
MYO5B	20	MYO5B,MYO5BP1,MYO5BP2, ENSG00000266997	20,2,2,5	PC,PG,PG,NMD
PCLAF	9	PCLAF,ENSG00000259316	9,1	PC,NMD
PDGFRA	29	PDGFRA,ENSG00000282278	29,9	PC,PC
PTGDS	5	PTGDS,ENSG00000284341	5,3	PC,NMD
SCD	20	SCD,SCDP1	20,3	PC,PG
SERHL2	8	SERHL2,SERHL	8,7	PC,PG
SERPINA3	27	SERPINA3,ENSG00000273259	27,14	PC,NMD
SLAMF1	24	SLAMF1,ENSG00000228863	23,1	PC,lncRNA
SMS	17	SMS,ENSG00000213080,ENSG00000249779, ENSG00000232389,ENSG00-000251342	17,7,1,3,1	PC,PG,PG,PG,PG
SVIL	20	SVIL,SVIL2P	20,2	PC,PG
THAP2	25	THAP2,ENSG00000258064	25,2	PC,NMD
TPD52	21	TPD52,ENSG00000276418	21,5	PC,NMD
TPSAB1	2	TPSAB1,TPSB2,TPSD1	2,2,1	PC,PC,PC
TRAF4	14	TRAF4,ENSG00000225869	14,1	PC,PG,PG,NMD
TUBA4A	12	TUBA4A,TUBA4B	12,1	PC,PC
TUBB2B	11	TUBB2B,TUBB2BP1,TUBB2A,TUBB4A,TUBB3, ENSG00000198211	11,2,3,1,1, 1	PC,PC,PC,PC,PG,PC
VOPP1	24	VOPP1,ENSG00000223612	24,1	PC,PG
VWF	20	VWF,VWFP1,LINC01665	20,2,1	PC,PG,lncRNA
ZEB2	47	ZEB2,ZEB2P1	47,1	PC,PG
ZNF562	22	ZNF562,ENSG00000291231,ZNF812P	22,3,3	PC,lncRNA,PG

112 **Table 1. OPT output of genes with predicted off-target binding based on perfect sequence**
113 **homology in GENCODE v47.** This table shows the 45 genes whose probes in the 10x Genomics
114 Xenium v1 Human Breast Gene Expression Panel exhibit predicted off-target probe binding,
115 where each off-target alignment involves a perfect 40bp match to the probe sequence. Although
116 OPT predicted off-target binding of CCPG1 probe sequences to the DNAAF1-CCPG1 gene, we
117 manually excluded it from our list because DNAAF1-CCPG1 is a read-through gene containing
118 portions of both DNAAF1 and CCPG1. The final column shows the gene types, in order, of each
119 of the off-target genes shown in column 3. Abbreviations: PC = protein-coding; PG = pseudogene;
120 NMD = nonsense-mediated decay; lncRNA = long non-coding RNA.
121
122
123 Variation in off-target binding predictions across different annotations
124
125 OPT relies on alignments to an annotated transcriptome, which ideally reflects all genes and gene
126 variants stably transcribed in a given species. However, genome annotation is still an active area
127 of research (Varabyou et al. 2023), with discrepancies across annotations in gene counts,
128 isoforms, and many other features. We therefore further used OPT to predict for off-target
129 binding and affected genes using two additional human genome annotation sets, RefSeq (v110),
130 (O'Leary et al. 2016) and CHESS (v3.1.3) (Varabyou et al. 2023), and compared to our previous
131 results from GENCODE (v47) (Mudge et al. 2025) (Methods).
132

133 When considering only perfect sequence homology, while we previously found 45 affected genes
134 using GENCODE, we found 22 when using RefSeq and 33 when using CHESS (Supplementary Table
135 1, 2). Given that RefSeq and CHESS have more transcripts than GENCODE, these discrepancies in
136 off-target binding predictions was not simply an artifact of the difference in transcript set sizes.
137
138 While the human annotation databases mostly agree on the number of protein-coding genes in
139 the genome, they remain widely divergent on pseudogenes and lncRNA genes. Therefore, we
140 focused on how the results change when we restrict our analysis to only protein-coding genes.
141 By excluding pseudogenes (which are presumably not expressed), lncRNAs, and other non-
142 protein-coding RNAs when using OPT, the number of affected genes fell to 17 for GENCODE and
143 RefSeq and 16 for CHESS (Supplementary Table 3). Again, these discrepancies reflect annotation
144 differences. For example, the probe sequence (ENSG00000196154|S100A4|ab4e3dc), which was
145 designed to target *S100A4* based on GENCODE annotations, also aligns to *S100A5* in RefSeq
146 (Supplementary Figure 1A). We reason that if a probe sequence aligns off-target to a protein-
147 coding gene based on any of these annotations, it could result in off-target binding. We therefore
148 focused further analysis on the union of genes with predicted off-target binding to protein-coding
149 genes across the 3 annotations, resulting in 21 genes: *ADGRE5*, *ADH1B*, *AKR1C1*, *AKR1C3*,
150 *APOBEC3A*, *APOBEC3B*, *AQP1*, *C1QA*, *CD79B*, *CEACAM6*, *FCGR3A*, *FLNB, KLRC1*, *KRT6B*, *PDGFRA*,
151 *S100A4, TOMM7, TPD52, TPSAB1*, *TUBA4A*, *TUBB2B* (Supplementary Table 4).
152
153

154 Comparison with Visium CytAssist reveals spatial gene expression patterns consistent with off-
155 target binding
156
157 To investigate the potential effects of our predicted off-target binding for the Xenium v1 Human
158 Breast Gene Expression Panel in experimental settings, we compared spatial gene expression
159 patterns detected in two previously published spatial transcriptomics datasets from serial
160 sections of the same breast cancer tissue: one section assayed with Xenium using the Xenium v1
161 Human Breast Gene Expression Panel, and another assayed using Visium CytAssist, an orthogonal
162 spatial transcriptomics platform (Janesick et al. 2023). Briefly, Visium is a sequencing-based
163 spatial transcriptomics technology in which RNA is hybridized to spatially barcoded capture spots
164 on a slide, enabling spatial transcriptomic mapping after sequencing. However, while Xenium
165 offers single-cell resolution gene expression quantification, Visium quantifies gene expression
166 within 55μm spots. To enable direct comparison, we first structurally aligned the Xenium and
167 Visium tissue sections using STalign (Clifton et al. 2023), restricting our analysis to overlapping
168 regions since different parts of the tissue were profiled (Supplementary Figure 2A). To enhance
169 visual comparison, we aggregate the Xenium gene expression data at these aligned locations to
170 match the Visium resolution (Supplementary Figure 2B) (Methods).
171
172 Among the 21 genes exhibiting off-target binding to protein-coding genes, 12 were present in
173 the Visium dataset that had at least one corresponding off-target gene also detected in the
174 dataset. For genes with no predicted off-target binding based on perfect sequence homology
175 such as *MS4A1*, we observed a visually similar spatial pattern between the two technologies

176 (Figure 2A), suggesting that spatially aligned groups of cells across the two technologies express
177 this gene at comparable relative magnitudes. However, for genes with predicted off-target
178 binding based on perfect sequence homology such as *TUBB2B*, we observed a visually dissimilar
179 spatial pattern between the two technologies (Figure 2B). Importantly, its predicted off-target
180 gene, *TUBB2A*, in Visium shows a visually more similar spatial pattern to the Xenium *TUBB2B*. To
181 better visualize the effect of off-target binding within the Xenium data, we aggregated the
182 expression of each gene along with its predicted off-targets found in the Visium dataset and
183 visually compared across spatial locations. Notably, the spatial pattern of the aggregated
184 expression of *TUBB2B* and *TUBB2A* in Visium is visually more similar to the spatial pattern of
185 *TUBB2B* in Xenium, consistent with the prediction that Xenium *TUBB2B* probes exhibit off-target
186 binding to *TUBB2A*. We further visually confirmed using the Integrative Genomics Viewer (IGV)
187 that a probe sequence intending to bind to *TUBB2B* also perfectly aligns to a sequence in *TUBB2A*,
188 consistent across all annotations evaluated (Supplementary Figure 1B).
189
190 Overall, when comparing the total gene expression between the two technologies, we observed
191 a generally strong positive correlation, consistent with the previously published work (Janesick
192 et al. 2023). We do not observe an obvious trend between gene expression magnitude and the
193 presence of predicted off-target probes (Figure 2C), suggesting that off-target binding prediction
194 alone does not explain the observed higher expression magnitude in Xenium compared to
195 Visium, which may still be attributed to variation in detection efficiency, sequencing depth, and
196 other factors.

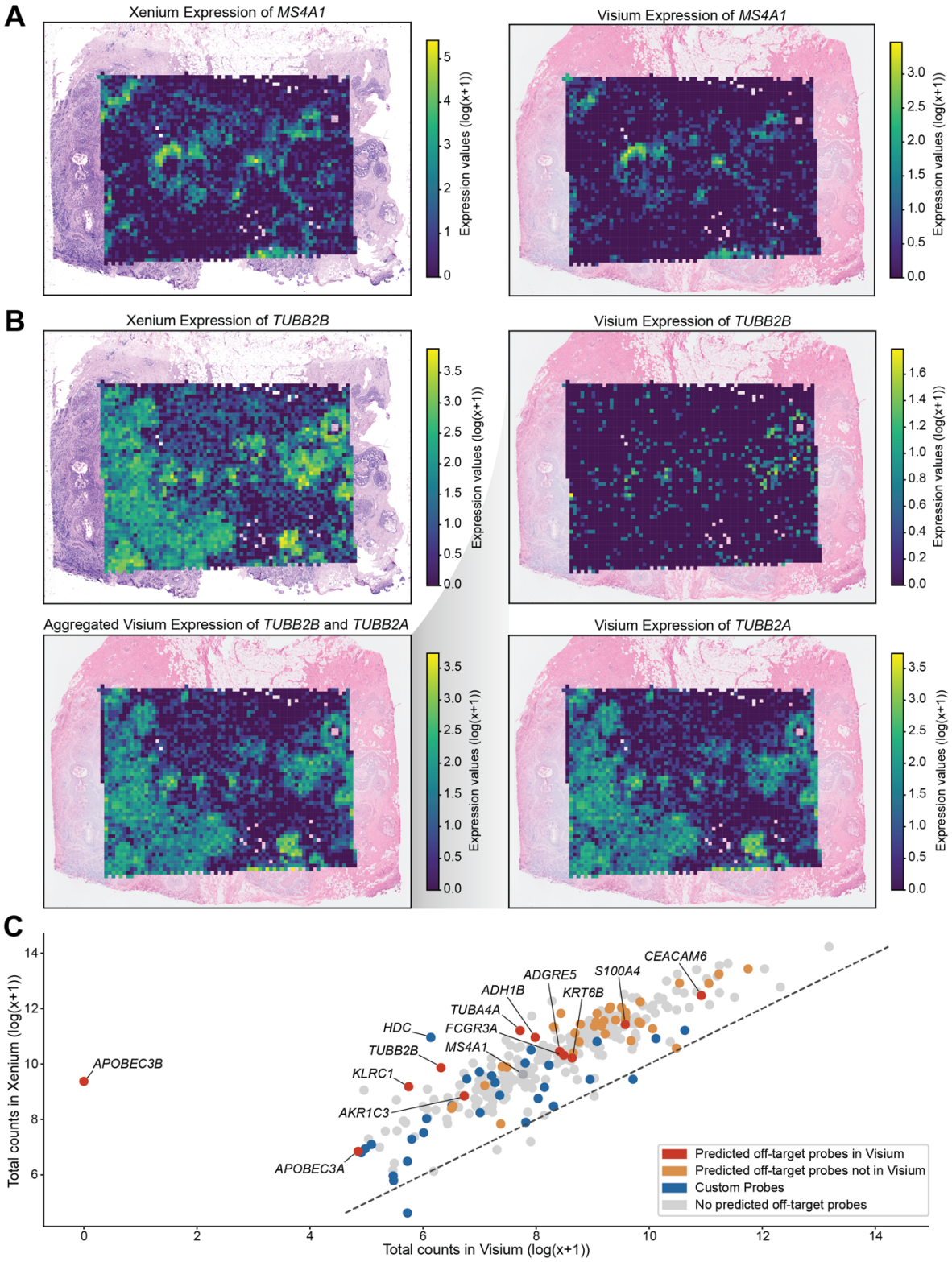

197

198 **Figure 2. Comparison of spatial gene expression patterns between Xenium and Visium. (A)**

199 Spatial gene expression of *MS4A1* overlaid on the corresponding histological images for Xenium

200 and Visium. **(B)** Gene expression patterns for *TUBB2B*: Xenium expression, Visium expression, the
201 aggregated Visium expression combining *TUBB2B* and its predicted off-target gene's expression
202 *TUBB2A*, and Visium expression of *TUBB2B*'s predicted off-target *TUBB2A*. (**C)** Scatterplot of log-
203 transformed total expression counts (with a pseudocount) for 307 genes comparing Visium and
204 Xenium data. The dotted line represents X = Y, and points (genes) are colored by probe
205 information.
206
207
208 <u>Comparison with scRNA-seq reveals single-cell gene expression patterns consistent with off-</u>
209 <u>target binding</u>
210
211 To further investigate the potential effects of our predicted off-target binding for Xenium probes,
212 we compared the detected single-cell gene expression patterns in the same previously published
213 work: again, the one assayed with Xenium using the Xenium v1 Human Breast Gene Expression
214 Panel, and another assayed using Chromium Next GEM Single Cell 3' (Janesick et al. 2023). Briefly,
215 single-cell RNA sequencing (scRNA-seq) with 3' end capture is a technique used to profile gene
216 expression at the single-cell level by profiling the 3' ends of mRNA transcripts with sequencing
217 followed by alignment to a genome or transcriptome for quantification. While this approach
218 provides single-cell resolution gene expression quantification, it lacks spatial information. To
219 enable a single-cell comparison with Xenium, we use Harmony (Korsunsky et al. 2019) to remove
220 batch effects and project cells into a shared UMAP embedding (Supplementary Figure 3)
221 (Methods).

222

223 Among the 21 genes exhibiting off-target binding to protein-coding genes, 16 were present in
224 the sc-RNAseq dataset that had at least one corresponding off-target gene also detected in the
225 dataset. Again, for genes with no predicted off-target binding based on perfect sequence
226 homology such as *MS4A1*, we observed a visually similar gene expression pattern in the
227 harmonized UMAP across both technologies (Figure 3A), suggesting that transcriptionally similar
228 clusters of cells or cell-types across the two technologies express this gene at comparable relative
229 magnitudes. Likewise, again, for genes with predicted off-target binding based on perfect
230 sequence homology such as *TUBB2B*, we observed a visually dissimilar gene expression pattern
231 on the harmonized UMAP (Figure 3B). Again, its predicted off-target gene, *TUBB2A,* in scRNA-seq
232 showed a visually more similar expression pattern in the harmonized UMAP embedding to the
233 Xenium *TUBB2B*. To better illustrate the impact of the off-target probes, we again aggregated
234 the expression of a gene and its predicted off-target genes present in the scRNA-seq data and
235 visually compared across the harmonized UMAP embedding. The aggregated expression of
236 *TUBB2B* and *TUBB2A* in the scRNA-seq data shows a visually more similar gene expression
237 pattern in the harmonized UMAP embedding to *TUBB2B* in the Xenium, consistent with the
238 prediction that Xenium *TUBB2B* probes exhibit off-target binding with these paralogs (Figure 3B,
239 Supplementary Figure 4).

240

241 Overall, when comparing total gene expression between the two technologies, we again
242 observed a generally strong positive correlation (Figure 3C), similar to the Visium comparison
243 results and consistent with the previously published work (Janesick et al. 2023).

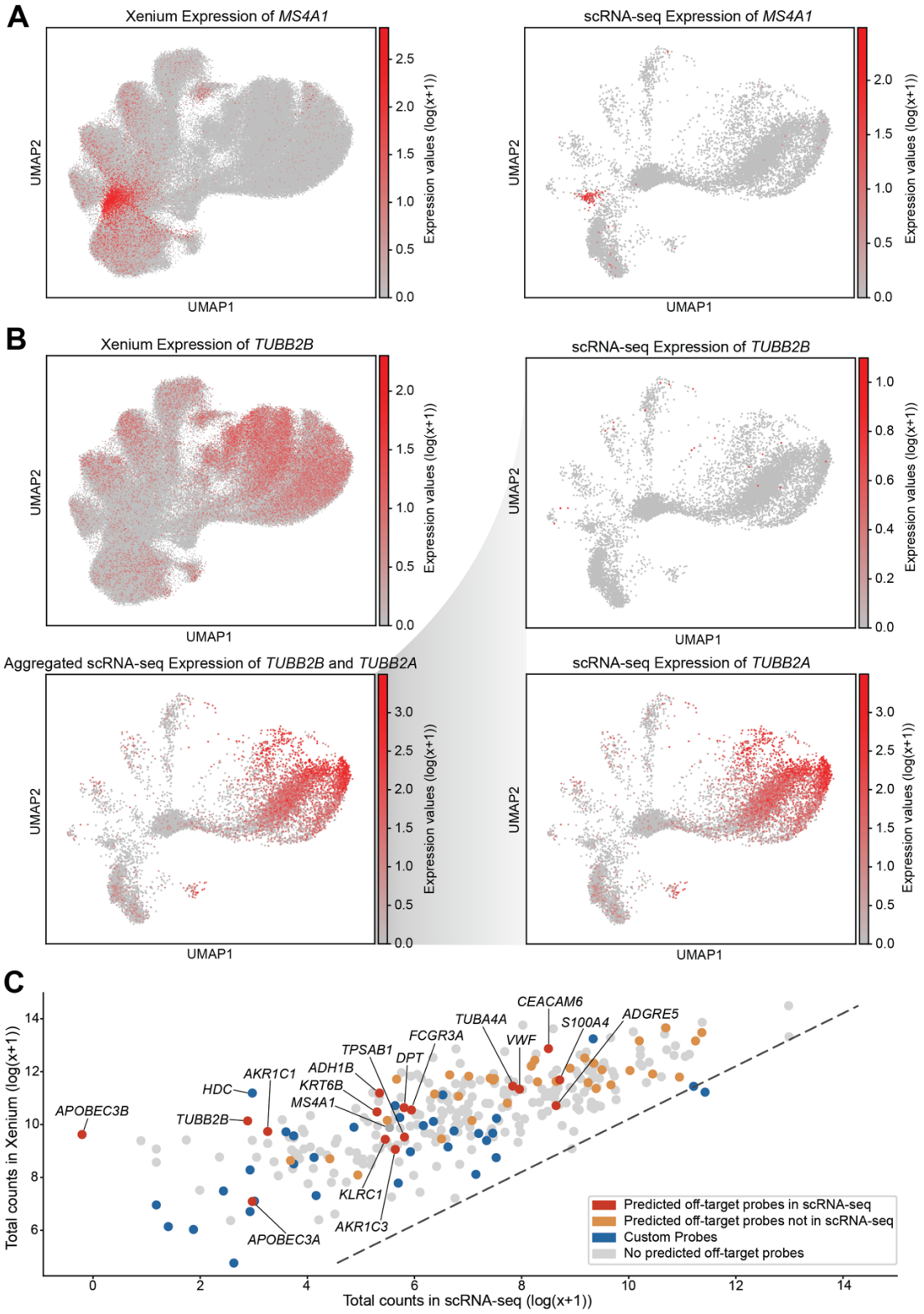

Figure 3. Comparison of single-cell gene expression patterns between Xenium and scRNA-seq. **(A)** Harmonized UMAP visualization of *MS4A1* expression for Xenium and scRNA-seq data. **(B)**

247 Comparison of *TUBB2B* expression patterns on harmonized UMAP: Xenium expression, scRNA-
248 seq expression, an aggregated scRNA-seq profile combining *TUBB2B* and its predicted off-target
249 gene's expression *TUBB2A*, and scRNA-seq expression of *TUBB2B*'s potential off-target *TUBB2A*.
250 Note that *TUBB2B* also has two additional off-targets present in the scRNA-seq data
251 (Supplementary Figure 4). **(C)** Scatterplot of log-transformed total expression counts (with a
252 pseudocount) for 313 genes between Visium and scRNA-seq data. The dotted line represents X =
253 Y, and points (genes) are colored by probe information.
254
255
256 <u>OPT results when allowing mismatches at the terminal ends of the probe sequences identifies</u>
257 <u>additional off-target candidates</u>
258
259 Thus far, we have focused on predicting off-target binding based on perfect sequence homology.
260 However, we reason that imperfect sequence matching could still result in off-target binding.
261 Specifically for the Xenium v1 Human Breast Gene Expression Panel, padlock probes with two 20
262 base pair (bp) arms bind complementary mRNA regions, forming a 40bp probe sequence. A ligase
263 then circularizes the padlock probe, favoring specific 2-bp junctions. Importantly, if there is a
264 sequence mismatch, particularly outside the ligation site towards the terminal ends of the probe
265 sequence, hybridization may still occur and result in off-target binding, albeit with reduced
266 hybridization efficiency (Supplementary Figure 5A). We therefore added an option in OPT to
267 allow imperfect alignments at the ends of the probe sequences, specifying the sequence length
268 at either ends, where mismatches, insertions, deletions, or clipping can occur (Methods).

Allowing for 6bp mismatches on either end of the 40bp probe sequence (i.e., requiring a 28bp match covering the middle of the probe sequence including the ligation site) revealed nine additional genes with potential off-target binding when using GENCODE v47 (Supplementary Table 5). Additionally, 18 of the 45 genes previously predicted to be affected by off-target binding based on perfect sequence homology were now predicted to have additional off-target binding, either through the accumulation of new probes with predicted off-target binding or from the identification of additional predicted off-target genes (Supplementary Table 6). Among these additional genes included *CEACAM8*, for which we observed a visually dissimilar spatial pattern between Xenium and Visium (Supplementary Figure 6A). Furthermore, the spatial pattern of the aggregate of *CEACAM8* with its predicted off-target genes (*CEACAM5*, *CEACAM6*, *CEACAM7*, *PSG6*) in Visium more closely resembled the spatial pattern of *CEACAM8* in Xenium. Likewise, a similar trend is observed in the scRNA-seq comparison (Supplementary Figure 6B). Ultimately, these findings suggest that off-target binding, even with imperfect sequence matching, can contribute to the expression patterns observed in Xenium.

Discussion

Our study presents evidence of off-target probe binding that may distort gene expression profiles affecting at least 21 out of the 280 genes in the Xenium v1 Human Breast Gene Expression Panel. This finding is supported by spatial and single-cell comparative analyses using Xenium with serial

291 section datasets from Visium CytAssist and 3' single-cell RNA-seq respectively. Although we focus
292 here on the Xenium v1 Human Breast Gene Expression Panel from 10x Genomics, we do not
293 exclude the possibility that off-target binding may similarly affect other probe-based gene
294 detection approaches. To assist in the interpretation of existing probe-based gene expression
295 data as well as future probe design, we provide OPT as a software tool for predicting potential
296 off-target probe binding.
297
298 Although we have predicted off-target binding based on sequence alignment, its effect on gene
299 expression quantification may still vary. One reason is that the off-target protein-coding or non-
300 protein-coding gene may not be expressed. For example, although *CEACAM6* probes have
301 predicted off-target binding to *CEACAM3* based on perfect sequence homology, the sparse
302 expression of *CEACAM3* in both the Visium and scRNA-seq breast cancer data led to only a minor
303 difference in the aggregated expression (Supplementary Figure 7). As such, the extent of the
304 effect of off-target binding depends on the expression of the off-target gene and will therefore
305 vary across tissues. On the other hand, self-hybridization or interactions between probes
306 themselves may occur to induce non-specific signals (Supplementary Fig 5B). In general, probe
307 binding specificity is influenced by numerous factors, with many methods previously developed
308 to aid in the design of probe sequences while taking these factors into consideration (Wang and
309 Seed 2003; Rouillard, Zuker, and Gulari 2003; Wernersson and Nielsen 2005; Chou 2010; Li et al.
310 2011; Hu et al. 2020; Hershberg et al. 2021; Fornace et al. 2022).
311

312 Notably, our evaluation was limited to the base 280-gene Xenium v1 Human Breast Gene
313 Expression Panel even though the expression of 313 total genes were quantified in these datasets
314 from Janesick et al. This is because 33 of the 313 targeted genes were probed using custom
315 sequences that were not publicly disclosed. Our comparative analysis suggests that *HDC*, a gene
316 with custom probe sequences mentioned in the paper, may also be subject to off-target binding.
317 In Xenium, *HDC* exhibited a distinct spatial pattern and high global expression level, whereas both
318 Visium and scRNA-seq data showed a minimal spatial pattern and sparse expression level
319 respectively (Supplementary Figure 8). We therefore speculate that *HDC* probes may exhibit off-
320 target binding but cannot fully validate without the probe sequences used for *HDC*. As such, we
321 emphasize the importance of publishing full probe sequences to enable reproducible science.
322
323 We also observed that 34 / 4,809 breast panel probe sequences did not align to any reference
324 transcripts in the GENCODE v47 annotation. 33 of these unmapped probe sequences matched
325 intronic sequences, which would not normally appear in mature transcripts. We manually aligned
326 the one remaining probe sequence (ENSG00000198851|CD3E|02369ef) to the GRCh38 genome
327 and found that it matched to chr11: 118304577 – 118304616, an intergenic region just upstream
328 of *CD3E*, the target gene for this probe. We suspect that these intron and intergenic panel probe
329 sequences were designed using an earlier version of the GENCODE annotation in which those
330 regions were annotated as exonic. This finding illustrates the importance of disclosing the specific
331 annotation version to promote reproducibility, as well as the ongoing variability of human gene
332 annotation. Likewise, as evidenced by our analysis across GENCODE, RefSeq, and CHESS, we
333 emphasize the variation across these reference annotations and therefore recommend

334 evaluating probe sequences for off-target effects using multiple annotations to be more
335 comprehensive.
336
337 Given these challenges, we advise probes with predicted off-target binding to protein-coding
338 genes based on perfect sequence homology be discarded in future experiments. Likewise, we
339 encourage the use of tools like OPT to aid in future probe design decisions and help ensure that
340 probes are optimized to minimize off-target binding based on current transcriptome annotations.
341 For datasets that have already been generated using probes with predicted off-target binding,
342 we generally recommend taking into consideration these predictions to avoid drawing misleading
343 conclusions. For example, we recommend expression measurements for genes with predicted
344 off-target binding be omitted from training foundation models to avoid error propagation.
345 Alternatively, when performing integrative analyses that compare or align gene expression with
346 measurements across technologies, it may be necessary to incorporate off-target binding
347 predictions. For example, integration could be performed between the observed Xenium gene
348 expression and the aggregated expression of the target and predicted off-target genes for the
349 orthogonal technology. Finally, existing literature that base conclusions on genes with predicted
350 off-target binding should be interpreted with caution.
351
352 We emphasize that these findings were missed in the previous Janesick et al. publication from
353 10x Genomics (Janesick et al. 2023). Consistent with previously published observations, we
354 observed a highly correlated total gene expression magnitude between Xenium and Visium as
355 well as scRNA-seq. However, a notable exception is *APOBEC3B*, which is not expressed according

356 to both Visium and scRNA-seq but highly expressed according to Xenium (Supplementary Figure
357 9) – a discrepancy that Janesick et al. omitted. We emphasize that positive significant average
358 gene expression correlation is a necessary but not sufficient metric for consistency across
359 technologies and that individual data points should be scrutinized. Likewise, validation with
360 orthogonal technologies could have helped identify discrepancies suggestive of off-target effects.
361 We note Janesick et al. only use immunofluorescence to validate two genes, *ERBB2* and *MS4A1*,
362 which by our analysis were predicted to exhibit no off-target binding. We therefore stress the
363 importance of more thorough orthogonal validations. Although Xenium incorporates blank and
364 negative control probes that are intended to help quantify the rate of non-specific and potential
365 off-target binding, our findings suggest that relying solely on such probes for error detection may
366 be insufficient. Implementing probe redundancy, where the same gene is targeted using different
367 codewords, could provide an additional internal control to enable the detection of off-target
368 binding.
369
370 This is not the first instance in which a commercially available platform has encountered
371 challenges in probe design (McCartney et al. 2016; Harbig 2005; Mecham et al. 2004; Liu, Bebu,
372 and Li 2014). These findings underscore the critical role of academic researchers towards
373 ensuring the robustness of industry-led product development by providing oversight, free of
374 financial conflicts of interest through independent federal funding. This complementarity
375 between industry and academia fosters a more rigorous, transparent, and reliable scientific
376 process, ultimately to the benefit of consumers and the public. By shedding light on putative off-
377 target probe binding as well as by providing a tool to enable such off-target binding predictions,

this work will help enhance the quality of spatial transcriptomics data and improve the overall reproducibility in spatial transcriptomics research.

Methods

Off-target Probe Tracker Tool (OPT)

OPT (Off-target Probe Tracker) is a Python program that runs nucmer (Marçais and Kingsford 2011) for alignment and then processes the results to predict probe binding based on sequence homology. OPT is available as an open-source Python toolkit at https://github.com/JEFworks-Lab/off-target-probe-tracker. When a user provides a query probe sequence file, a target transcript sequence file, and the annotation used to extract these transcripts, OPT outputs which gene each probe is likely to bind to. Nucmer is a fast nucleotide sequence aligner that uses maximal exact matches as anchors which it then joins together to find longer alignments. By default, OPT saves nucmer results in SAM format and finds perfect sequence matches between a query probe and a target transcript, requiring that alignments consist of only matches and cover the entirety of the query. OPT consists of three modules: (1) `flip` for reverse complementing probe sequences aligned to the opposite strand of their target genes; (2) `track` for aligning probe sequences and processing alignment results; and (3) `stat` for compiling summary statistics on the number of off-target binding probes and affected genes.

400 In the case that a probe's target gene has synonyms, we consider alignments to genes annotated
401 with one of its synonym to still be on-target. For example, if a probe that targets *NARS* shows
402 alignments to a gene called *NARS1*, we don't consider it to be off-target binding. We gathered
403 relevant gene synonym relationships using the GeneCards and HGNC online database.
404
405 OPT also provides a “pad” mode in which imperfect alignments are allowed at either end of the
406 query (i.e., probe sequence). The -pl parameter sets the pad length at either end of the query
407 and OPT allows for any number of mismatches in these padded regions. For example, if the pad
408 length is 6 and the probe sequence length is 40, then the middle 28bp are the only part of the
409 probe sequence required to match. As long as the critical region is intact, OPT reports an off-
410 target binding site based on this alignment. By default, -pl is set to 0, and the pad mode is
411 activated by providing a non-zero integer to -pl.
412
413
414 Obtaining probe sequences for the Xenium v1 Human Breast Gene Expression Panel
415
416 To identify potential off-target binding impacting the 10x Genomics Xenium v1 Human Breast
417 Gene Expression Panel, we obtained the FASTA file of probe sequences from the 10x Genomics
418 Website (https://cdn.10xgenomics.com/raw/upload/v1684948097/software-support/Xenium-
419 panels/hBreast_panel_files/xenium_human_breast_gene_expression_panel_probe_sequences.
420 fasta) and available as Supplementary Data for preservation.
421

422 The target gene name and ID was extracted from the probe IDs of the following format:

423

424 `> gene_id|gene_name|accession`

425

426 We expected the provided FASTA file to contain probe sequences to be the reverse
427 complemented sequence of their intended target genes and hence align to the reverse strand of
428 their target isoforms. However, when we aligned the breast panel probe sequences to the
429 GENCODE basic (v47) reference transcripts using nucmer, we found that only 2,508 / 4,809
430 (52.2%) of probe sequences aligned on the reverse strand of their target transcripts (i.e., isoforms
431 of their target genes). For consistency, we enforced that all probe sequences be oriented in the
432 same direction and align to the forward strand of their target genes and transcripts. As such, we
433 reverse-complemented these 2,508 probe sequences. We also added this functionality as an OPT
434 module called "flip" in which probe sequences aligned to the reverse strand of their targets are
435 reverse complemented. We expect probe sequences to align to the forward strand of transcripts
436 (i.e., both oriented in the same direction) during the downstream probe sequence binding
437 prediction step.

438

439 Visium Comparison

440

441 The Visium CytAssist dataset, collected from a breast cancer tissue block utilized in Janesick et
442 al., was downloaded from the 10x Genomics website
443 (https://www.10xgenomics.com/products/xenium-in-situ/preview-dataset-human-breast). This

444 dataset originally contained 4,992 spots with x-y coordinates and includes 18,085 genes per spot.
445 Six genes (*AKR1C1*, *ANGPT2*, *BTNL9*, *CD8B*, *POLR2J3*, *TPSAB1*) were excluded from the analysis
446 since they were not present in the Visium dataset.
447
448 To compare spatial gene expression patterns from Visium and Xenium technologies, we first
449 mapped all the data to the same coordinate space. We used STalign (v1.0.1), a computational
450 tool that utilizes affine transformations along with diffeomorphic metric mapping to align target
451 and source datasets (Clifton et al. 2023). The initial alignment involved only affine
452 transformations and eight manually determined landmarks to align the Visium histology image
453 (source) to the Xenium histology image (target). This transformation brought the Visium image
454 into the coordinate space of the higher-resolution Xenium image. We then applied this learned
455 transformation to the Visium spots, ensuring that they were correctly positioned relative to both
456 histology images. Next, we used STalign to map the Xenium transcripts (source) onto their
457 corresponding Xenium histology image (target) using both affine and diffeomorphic metric
458 mapping. The transcripts were rasterized at 30μm resolution, with an initial affine transformation
459 guided by four manually defined landmarks. Diffeomorphic metric mapping was then performed
460 with the following parameters: a = 2500, epV = 1, niter = 2000, sigmaA = 0.11, sigmaB = 0.10,
461 sigmaM = 0.15, sigmaP = 50, muA = [1, 1, 1], muB = [0, 0, 0], with all other settings left at their
462 defaults. We extracted the overlapping regions between the two datasets (Supplementary Figure
463 2A), which reduced the total spots in the Visium dataset to 3,958. Finally, we aggregated the
464 Xenium gene expression data to ~55μm x 55μm patches that correspond to the spatial locations

465 of the Visium spots, resulting in matched-resolution spatial gene expression for both
466 technologies (Supplementary Figure 2B).
467
468
469 Single-cell RNA-seq Comparison
470
471 The Chromium Next GEM 3' scRNA-seq dataset, collected from a breast cancer tissue block
472 utilized in Janesick et al., was downloaded from the 10x Genomics website
473 (https://www.10xgenomics.com/products/xenium-in-situ/preview-dataset-human-breast). This
474 dataset contained 12,388 cells with 36,601 genes per cell. All 313 unique genes present in the
475 Xenium dataset are also in the scRNA-seq data, hence both datasets were subsetted to these
476 genes for this analysis.
477
478 Both scRNA-seq and Xenium provide single-cell resolution data. To integrate these datasets, we
479 first removed cells lacking detectable gene expression. We the normalized the combined gene
480 expression data using counts per million (CPM) and applied a log transformation with a
481 pseudocount of 1. Principal component analysis (PCA) is then applied to the normalized data, and
482 batch effects are corrected using Harmony (v1.2.3) on the top 30 principal components (PCs)
483 using default parameters except for theta, which was set to 8, to promote further mixing with
484 clusters across technologies. Finally, Uniform Manifold Approximation and Projection (UMAP) is
485 performed on the harmonized PCs, generating a shared 2D embedding across the two

technologies, and the data is further facetted by technology for visualization (Supplementary Figure 3).

Cross-annotation analysis

To compare OPT's results with different reference annotations, we used the most recent releases of GENCODE basic (v47), GENCODE comprehensive (v47), RefSeq (v110), and CHESS (v3.1.3) annotation of the GRCh38 genome. Note that GENCODE "basic" is the more reliable version of the annotation and is much closer to RefSeq and CHESS. GENCODE "comprehensive" includes hundreds of thousands of low-quality annotations, which we included in some of our analyses for completeness. Note also that GRCh38 has many non-reference sequences called "alternative scaffolds"; we removed these for our analysis. We then used gffread to extract transcripts as defined in these annotations by running:

```
$ gffread -w transcripts.fa -g grch38.p12/14.fa annotation.gff
```

The GRCh38.p14 assembly was used during transcript sequence extraction for all reference annotations, except for CHESS which specifies that the annotation maps genes and transcripts onto the GRCh38.p12 assembly. For RefSeq, we renamed the VD(J) segment features as transcript features to ensure consistency, and we also removed transcript sequences with the gene_biotype "pseudogene." RefSeq has a separate biotype called "transcribed_pseudogene,"

508 but doesn't annotate transcripts for these features. We considered transcripts annotated for a
509 small subset of just pseudogenes an error in the annotation.
510
511
512 **Conflicting interests**
513 The authors declare no conflicting interests.
514
515
516 **Acknowledgements**
517 We thank Reza Kalhor for his input on the project and feedback on the manuscript. Research
518 reported in this publication was supported by the National Institute of General Medical Sciences
519 of the National Institutes of Health under Awards R35-GM142889 and R35-GM130151, and the
520 HuBMAP Integration, Visualization, and Engagement (HIVE) Initiative under Award Number OT2-
521 OD033760.
522
523
524
525

References

10x Genomics. 2025a. “10x Genomics Product Catalog.” March 19, 2025. www.10xgenomics.com/store/product-catalog?query=xenium.

———. 2025b. “TXG_Q4-and-Full-Year-2024-Earnings-Press-Release.” 10x Genomics Reports Fourth Quarter and Full Year 2024 Financial Results and Provides Outlook for 2025. March 19, 2025. https://s28.q4cdn.com/592666581/files/doc_financials/2024/q4/TXG_Q4-and-Full-Year-2024-Earnings-Press-Release.pdf.

Chou, Hui-Hsien. 2010. “Shared Probe Design and Existing Microarray Reanalysis Using PICKY.” *BMC Bioinformatics* 11 (1): 196. https://doi.org/10.1186/1471-2105-11-196.

Clifton, Kalen, Manjari Anant, Gohta Aihara, Lyla Atta, Osagie K. Aimiuwu, Justus M. Kebschull, Michael I. Miller, Daniel Tward, and Jean Fan. 2023. “STalign: Alignment of Spatial Transcriptomics Data Using Diffeomorphic Metric Mapping.” *Nature Communications* 14 (1): 8123. https://doi.org/10.1038/s41467-023-43915-7.

Fornace, Mark E., Jining Huang, Cody T. Newman, Nicholas J. Porubsky, Marshall B. Pierce, and Niles A. Pierce. 2022. “NUPACK: Analysis and Design of Nucleic Acid Structures, Devices, and Systems.” Chemistry. https://doi.org/10.26434/chemrxiv-2022-xv98l.

Harbig, J. 2005. “A Sequence-Based Identification of the Genes Detected by Probesets on the Affymetrix U133 plus 2.0 Array.” *Nucleic Acids Research* 33 (3): e31–e31. https://doi.org/10.1093/nar/gni027.

Hershberg, Elliot A., Conor K. Camplisson, Jennie L. Close, Sahar Attar, Ryan Chern, Yuzhen Liu, Shreeram Akilesh, Philip R. Nicovich, and Brian J. Beliveau. 2021. “Author Correction: PaintSHOP Enables the Interactive Design of Transcriptome- and Genome-Scale Oligonucleotide FISH Experiments.” *Nature Methods* 18 (10): 1265–1265. https://doi.org/10.1038/s41592-021-01273-6.

Hu, Mengwei, Bing Yang, Yubao Cheng, Jonathan S. D. Radda, Yanbo Chen, Miao Liu, and Siyuan Wang. 2020. “ProbeDealer Is a Convenient Tool for Designing Probes for Highly Multiplexed Fluorescence in Situ Hybridization.” *Scientific Reports* 10 (1): 22031. https://doi.org/10.1038/s41598-020-76439-x.

Janesick, Amanda, Robert Shelansky, Andrew D. Gottscho, Florian Wagner, Stephen R. Williams, Morgane Rouault, Ghezal Beliakoff, et al. 2023. “High Resolution Mapping of the Tumor Microenvironment Using Integrated Single-Cell, Spatial and in Situ Analysis.” *Nature Communications* 14 (1): 8353. https://doi.org/10.1038/s41467-023-43458-x.

Korsunsky, Ilya, Nghia Millard, Jean Fan, Kamil Slowikowski, Fan Zhang, Kevin Wei, Yuriy Baglaenko, Michael Brenner, Po-ru Loh, and Soumya Raychaudhuri. 2019. “Fast, Sensitive and Accurate Integration of Single-Cell Data with Harmony.” *Nature Methods* 16 (12): 1289–96. https://doi.org/10.1038/s41592-019-0619-0.

Li, Qiyuan, Nicolai J Birkbak, Balazs Gyorffy, Zoltan Szallasi, and Aron C Eklund. 2011. “Jetset: Selecting the Optimal Microarray Probe Set to Represent a Gene.” *BMC Bioinformatics* 12 (1): 474. https://doi.org/10.1186/1471-2105-12-474.

Liu, Hongfang, Ionut Bebu, and Xin Li. 2014. “Microarray Probes and Probe Sets.” *Front Biosci* 2 (1): 325–38. https://doi.org/10.2741/e93.

Marçais, Guillaume, Arthur L. Delcher, Adam M. Phillippy, Rachel Coston, Steven L. Salzberg, and Aleksey Zimin. 2018. “MUMmer4: A Fast and Versatile Genome Alignment System.” Edited by Aaron E. Darling. *PLOS Computational Biology* 14 (1): e1005944. https://doi.org/10.1371/journal.pcbi.1005944.

Marçais, Guillaume, and Carl Kingsford. 2011. “A Fast, Lock-Free Approach for Efficient Parallel Counting of Occurrences of *k* -Mers.” *Bioinformatics* 27 (6): 764–70. https://doi.org/10.1093/bioinformatics/btr011.

McCartney, Daniel L., Rosie M. Walker, Stewart W. Morris, Andrew M. McIntosh, David J. Porteous, and Kathryn L. Evans. 2016. “Identification of Polymorphic and Off-Target Probe Binding Sites on the Illumina Infinium MethylationEPIC BeadChip.” *Genomics Data* 9 (September):22–24. https://doi.org/10.1016/j.gdata.2016.05.012.

Mecham, Brigham H., Daniel Z. Wetmore, Zoltan Szallasi, Yoel Sadovsky, Isaac Kohane, and Thomas J. Mariani. 2004. “Increased Measurement Accuracy for Sequence-Verified Microarray Probes.” *Physiological Genomics* 18 (3): 308–15. https://doi.org/10.1152/physiolgenomics.00066.2004.

Mudge, Jonathan M, Sílvia Carbonell-Sala, Mark Diekhans, Jose Gonzalez Martinez, Toby Hunt, Irwin Jungreis, Jane E Loveland, et al. 2025. “GENCODE 2025: Reference Gene Annotation for Human and Mouse.” *Nucleic Acids Research* 53 (D1): D966–75. https://doi.org/10.1093/nar/gkae1078.

O’Leary, Nuala A., Mathew W. Wright, J. Rodney Brister, Stacy Ciufo, Diana Haddad, Rich McVeigh, Bhanu Rajput, et al. 2016. “Reference Sequence (RefSeq) Database at NCBI: Current Status, Taxonomic Expansion, and Functional Annotation.” *Nucleic Acids Research* 44 (D1): D733–45. https://doi.org/10.1093/nar/gkv1189.

Rouillard, J.-M., Micahel Zuker, and Erdogan Gulari. 2003. “OligoArray 2.0: Design of Oligonucleotide Probes for DNA Microarrays Using a Thermodynamic Approach.” *Nucleic Acids Research* 31 (12): 3057–62. https://doi.org/10.1093/nar/gkg426.

Varabyou, Ales, Markus J. Sommer, Beril Erdogdu, Ida Shinder, Ilia Minkin, Kuan-Hao Chao, Sukhwan Park, et al. 2023. “CHESS 3: An Improved, Comprehensive Catalog of Human Genes and Transcripts Based on Large-Scale Expression Data, Phylogenetic Analysis, and Protein Structure.” *Genome Biology* 24 (1): 249. https://doi.org/10.1186/s13059-023-03088-4.

Wang, Xiaowei, and Brian Seed. 2003. “Selection of Oligonucleotide Probes for Protein Coding Sequences.” *Bioinformatics* 19 (7): 796–802. https://doi.org/10.1093/bioinformatics/btg086.

Wernersson, R., and H. B. Nielsen. 2005. “OligoWiz 2.0--Integrating Sequence Feature Annotation into the Design of Microarray Probes.” *Nucleic Acids Research* 33 (Web Server): W611–15. https://doi.org/10.1093/nar/gki399.

Yahoo Finance. 2025. “10x Genomics, Inc. (TXG).” 10x Genomics, Inc. (TXG). March 19, 2025. https://finance.yahoo.com/quote/TXG/.

Supplementary Figures

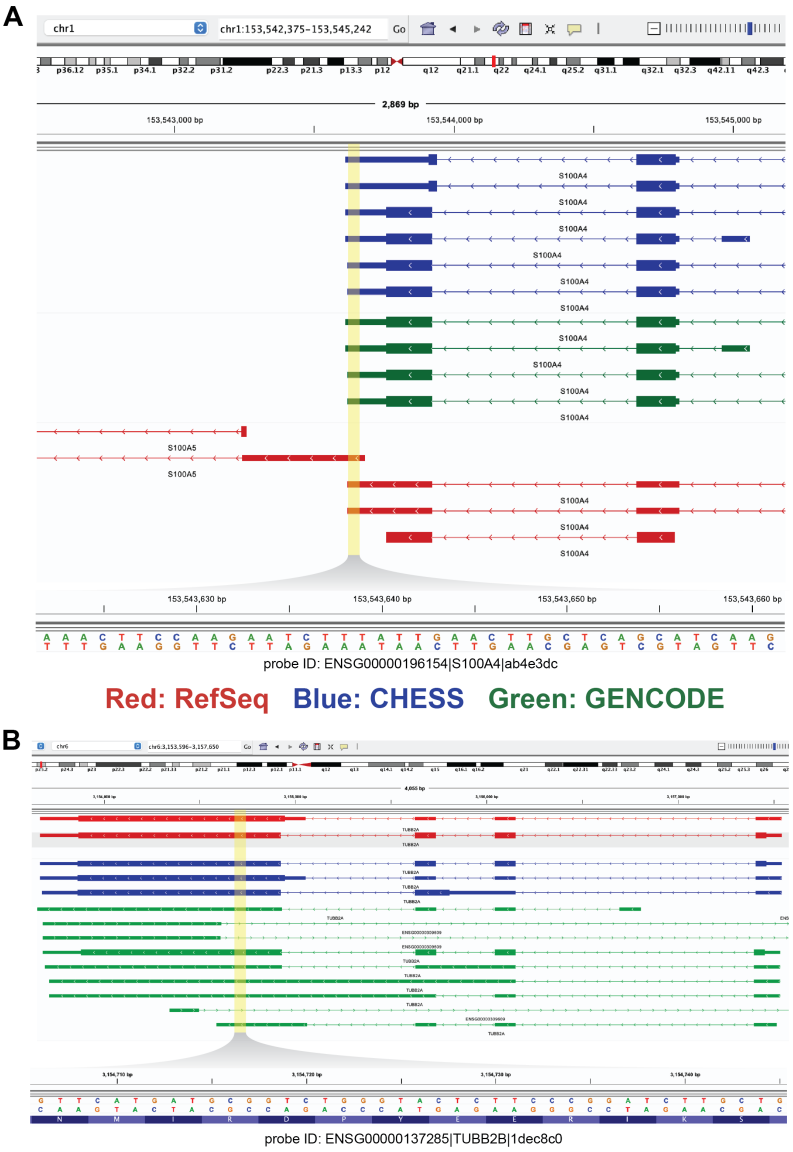

Supplementary Figure 1. (A) Screenshot from the Integrated Genome Viewer (IGV) showing the 40bp probe sequence (ID: ENSG00000196154|S100A4|ab4e3dc) that matches both *S100A5* and *S100A4*. Shown are 6 isoforms from the CHESS v3.1 annotation, 4 from GENCODE Basic v47, and 3 from RefSeq v110 for *S100A4*, as well as 2 RefSeq isoforms for the neighboring *S100A5*. The probe sequence aligns to the overlapping region between *S100A5* and *S100A4* gene loci. Matching probe shown in a zoomed-in view below. The forward- and reverse-strand sequences of the probe are shown, and the highlighted area indicates approximately where the probe falls within the gene. **(B)** Screenshot from the Integrated Genome Viewer (IGV) showing the 40bp probe sequence (ENSG00000137285|TUBB2B|1dec8c0) that matches both *TUBB2A* and *TUBB2B*. Shown are the 2 isoforms of *TUBB2A* from the RefSeq v110 annotation, 3 isoforms from the CHESS v3.1 annotation, and 9 from GENCODE Basic v47. Matching probe shown in a zoomed-in view below. The forward- and reverse-strand sequences of the probe are shown, and the highlighted area indicates approximately where the probe falls within the gene. **(A)** and **(B)** share a figure legend.

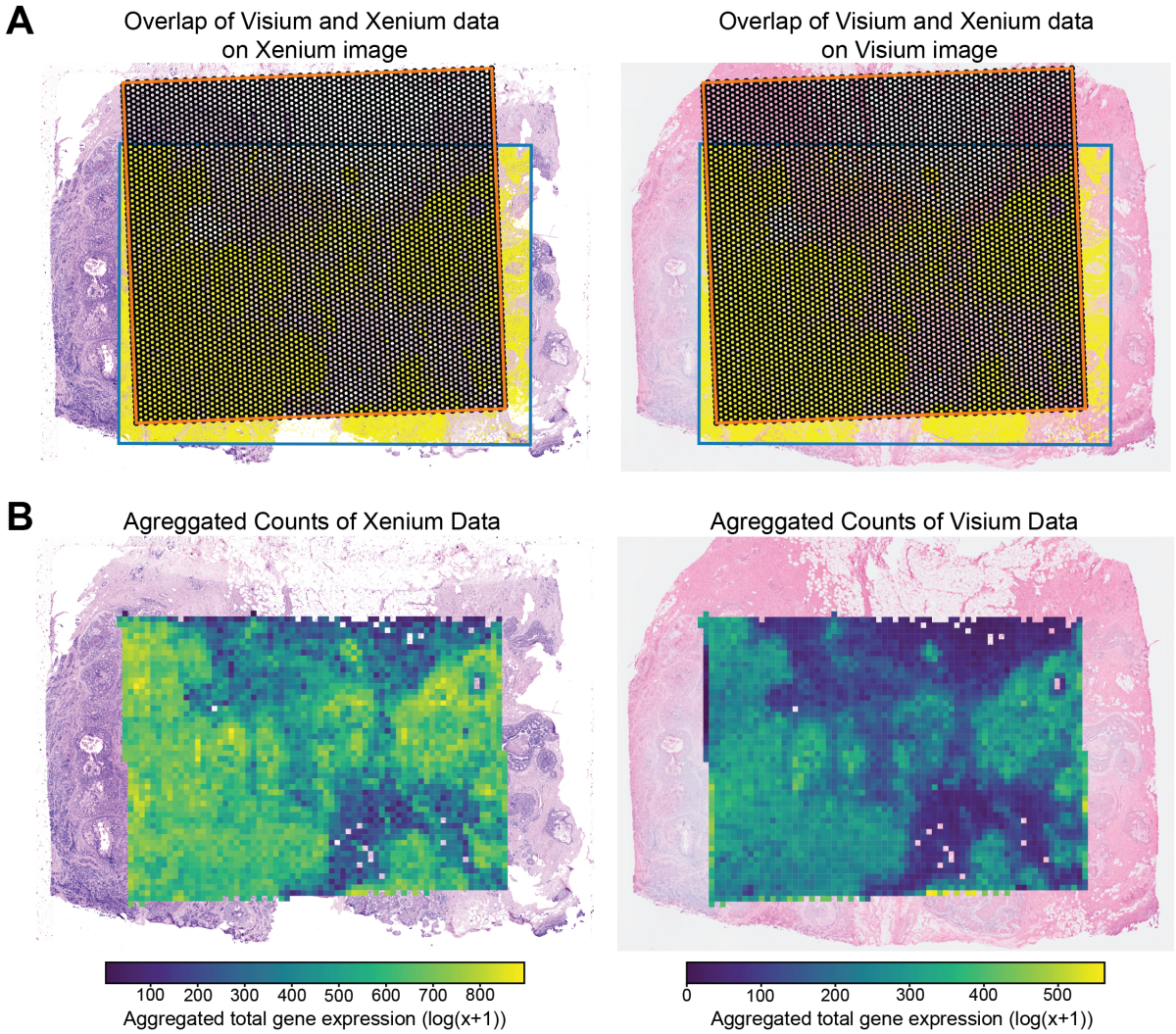

Supplementary Figure 2. (A) Overlap regions between Visium (orange outline) and Xenium (blue outline) data, shown on the Xenium histological image and the Visium histological image, respectively. **(B)** Log transformed aggregated total gene counts for spots (~55μm x 55μm) in both Xenium and Visium datasets, overlaid on their corresponding histological image.

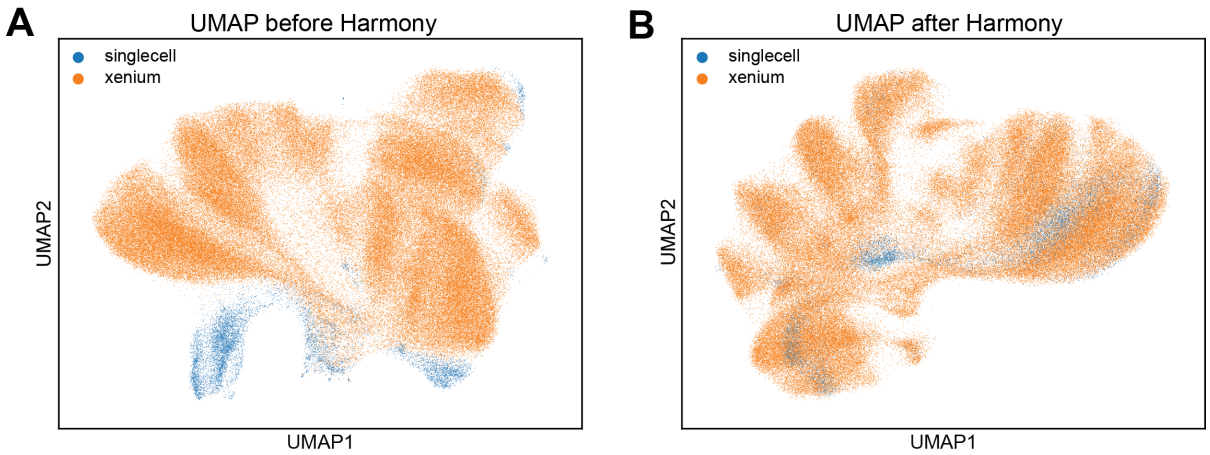

Supplementary Figure 3. UMAP visualization of integrated scRNA-seq and Xenium datasets: **(A)** before harmony batch correction and **(B)** after harmony batch correction.

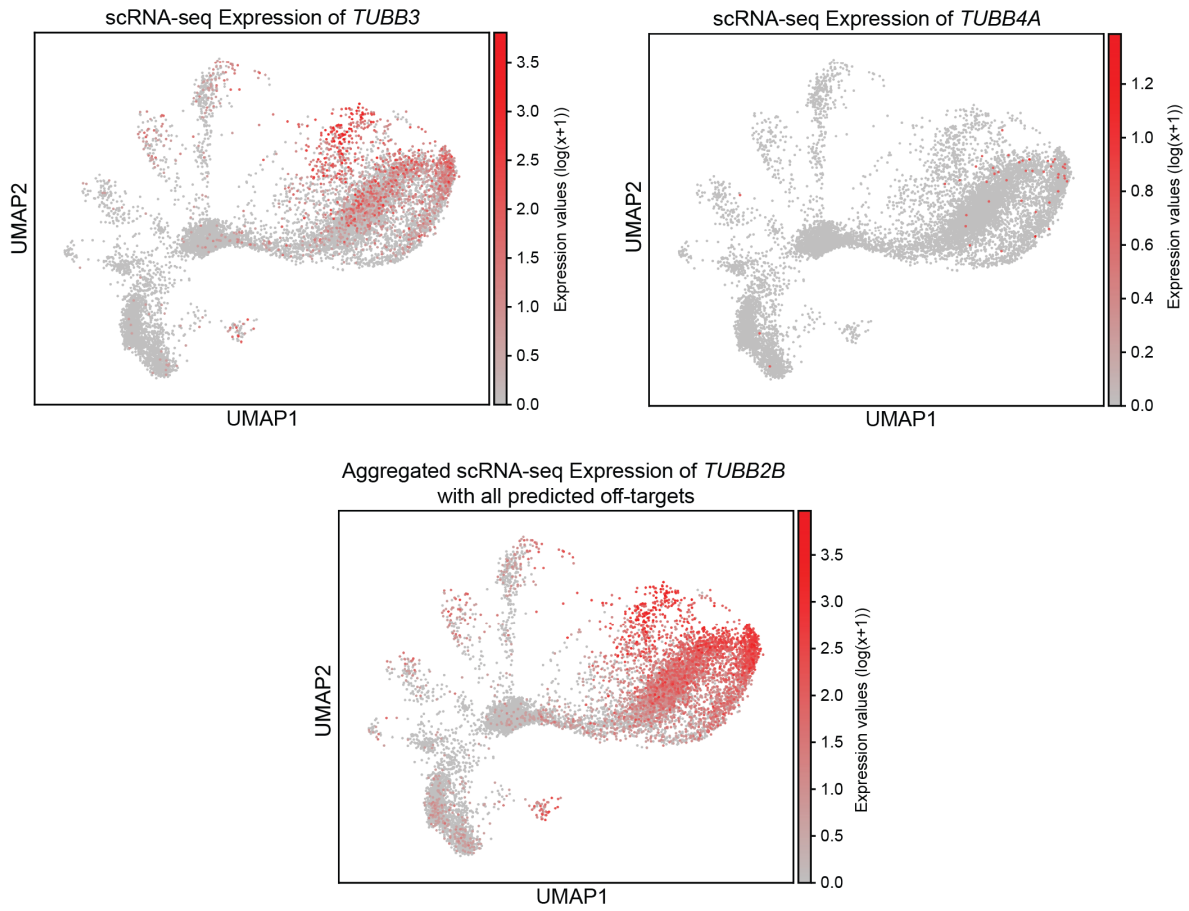

Supplementary Figure 4. Harmonized UMAP visualization of *TUBB3* and *TUBB4A* expression in the scRNA-seq dataset, as well as the aggregated scRNA-seq expression of *TUBB2B* and all predicted off-targets (*TUBB2A*, *TUBB3*, *TUBB4A*).

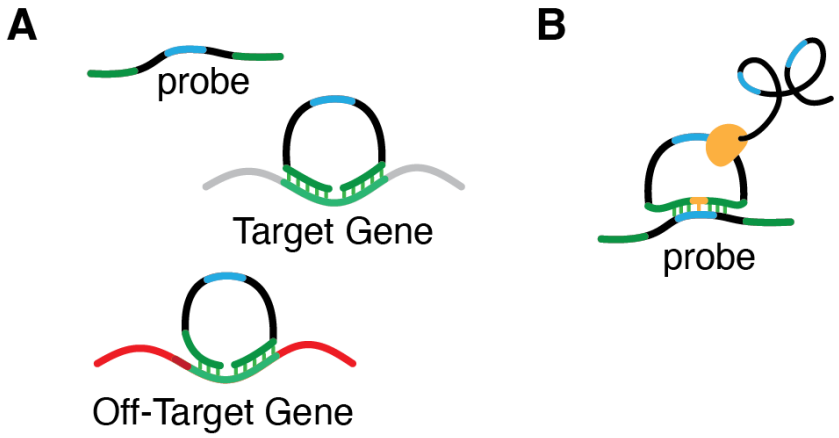

Supplementary Figure 5. (A) Schematic illustrating that hybridization may still occur even when there is a sequence mismatch at the non-ligated ends of the probe sequence. **(B)** Schematic depicting how probes could bind to each other instead of to their intended target.

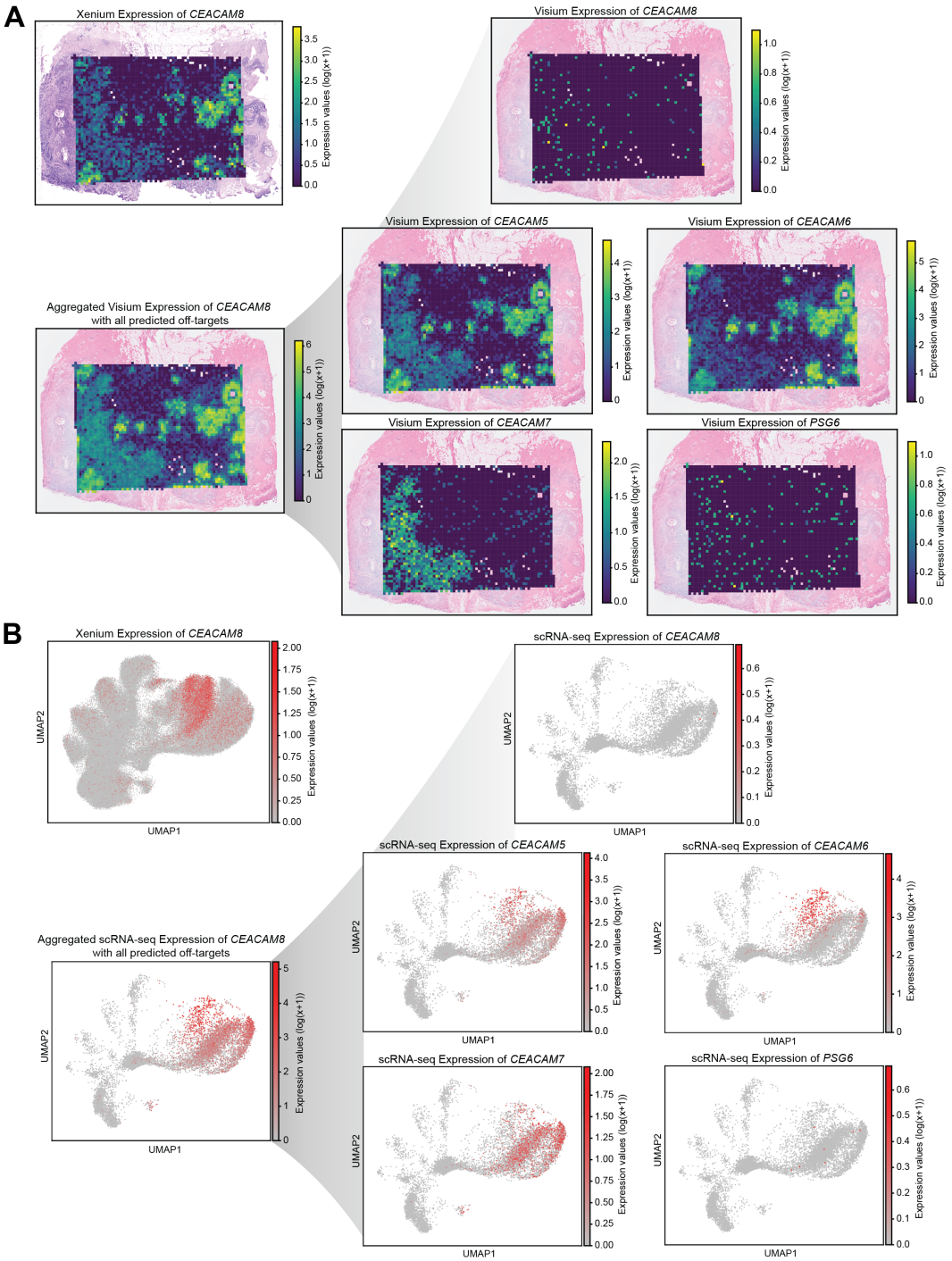

Supplementary Figure 6. (A) Spatial gene expression patterns for *CEACAM8*: Xenium expression, Visium expression, the aggregated Visium expression combining *CEACAM8* with all predicted off-target binding gene expression, and Visium expression of *CEACAM8*'s potential off-targets (*CEACAM5*, *CEACAM6*, *CEACAM7*, and *PSG6*). **(B)** Comparison of *CEACAM8* expression patterns on harmonized UMAP: Xenium expression, scRNA-seq expression, an aggregated scRNA-seq profile combining *CEACAM8* with all predicted off-target binding gene expression, and scRNA-seq expression of *CEACAM8*'s potential off-targets (*CEACAM5*, *CEACAM6*, *CEACAM7*, and *PSG6*).

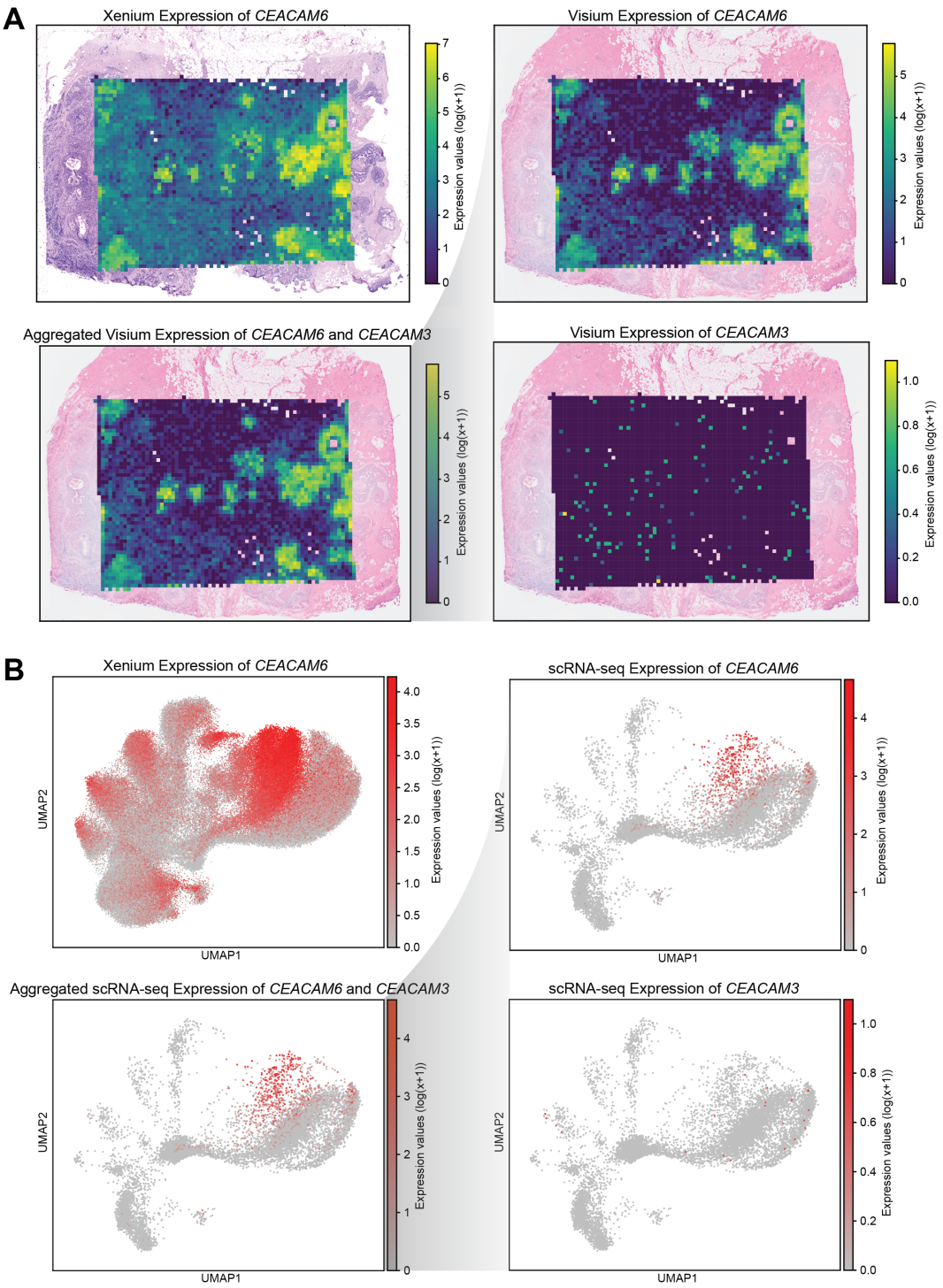

Supplementary Figure 7. (A) Spatial gene expression patterns for *CEACAM6*: Xenium expression, Visium expression, the aggregated Visium expression combining *CEACAM6* with all predicted off-target binding gene expression, and Visium expression of *CEACAM6* potential off-target (*CEACAM3*). **(B)** Comparison of *CEACAM6* expression patterns on harmonized UMAP: Xenium expression, scRNA-seq expression, an aggregated scRNA-seq profile combining *CEACAM6* with all predicted off-target binding gene expression, and scRNA-seq expression of *CEACAM6*'s potential off-target (*CEACAM3*).

637

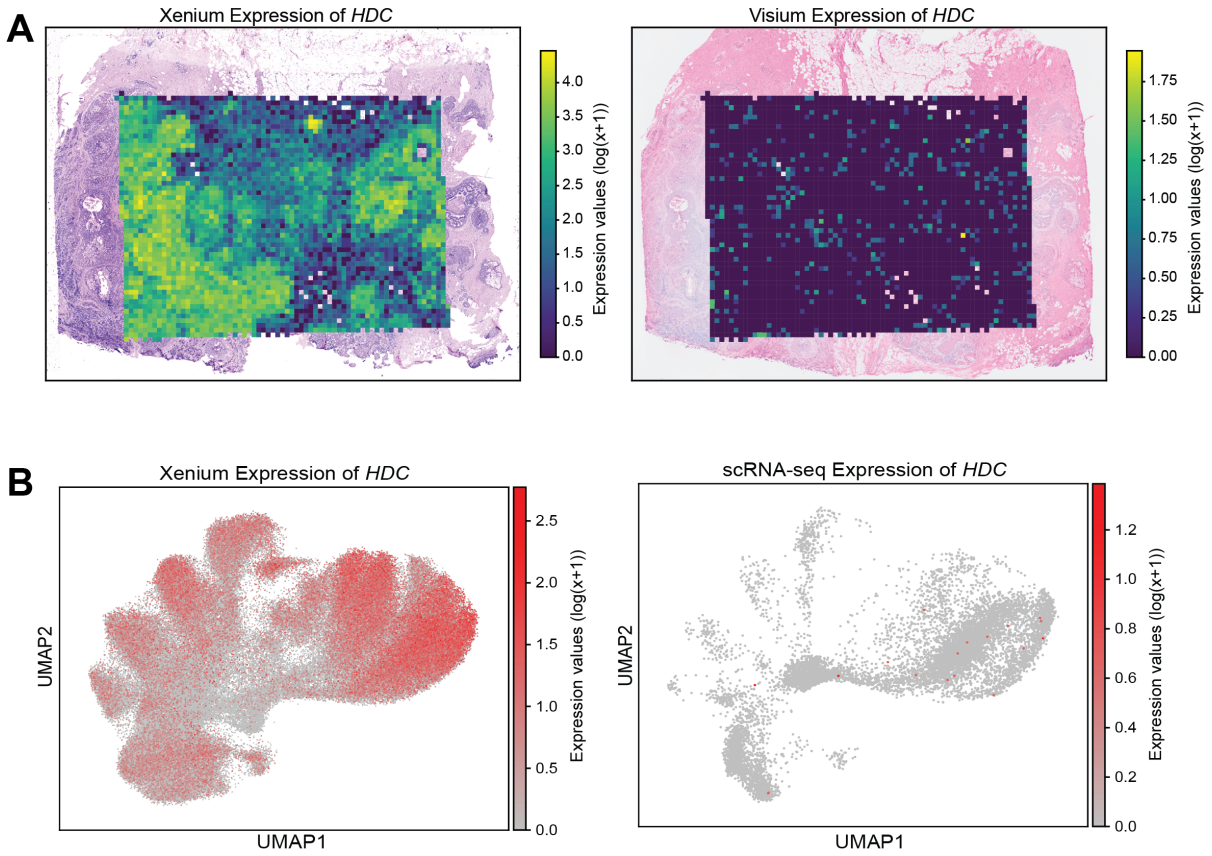

Supplementary Figure 8. (A) Spatial gene expression of *HDC* overlaid on the corresponding histological images for Xenium and Visium. **(B)** Harmonized UMAP visualization of *HDC* expression for Xenium and scRNA-seq data.

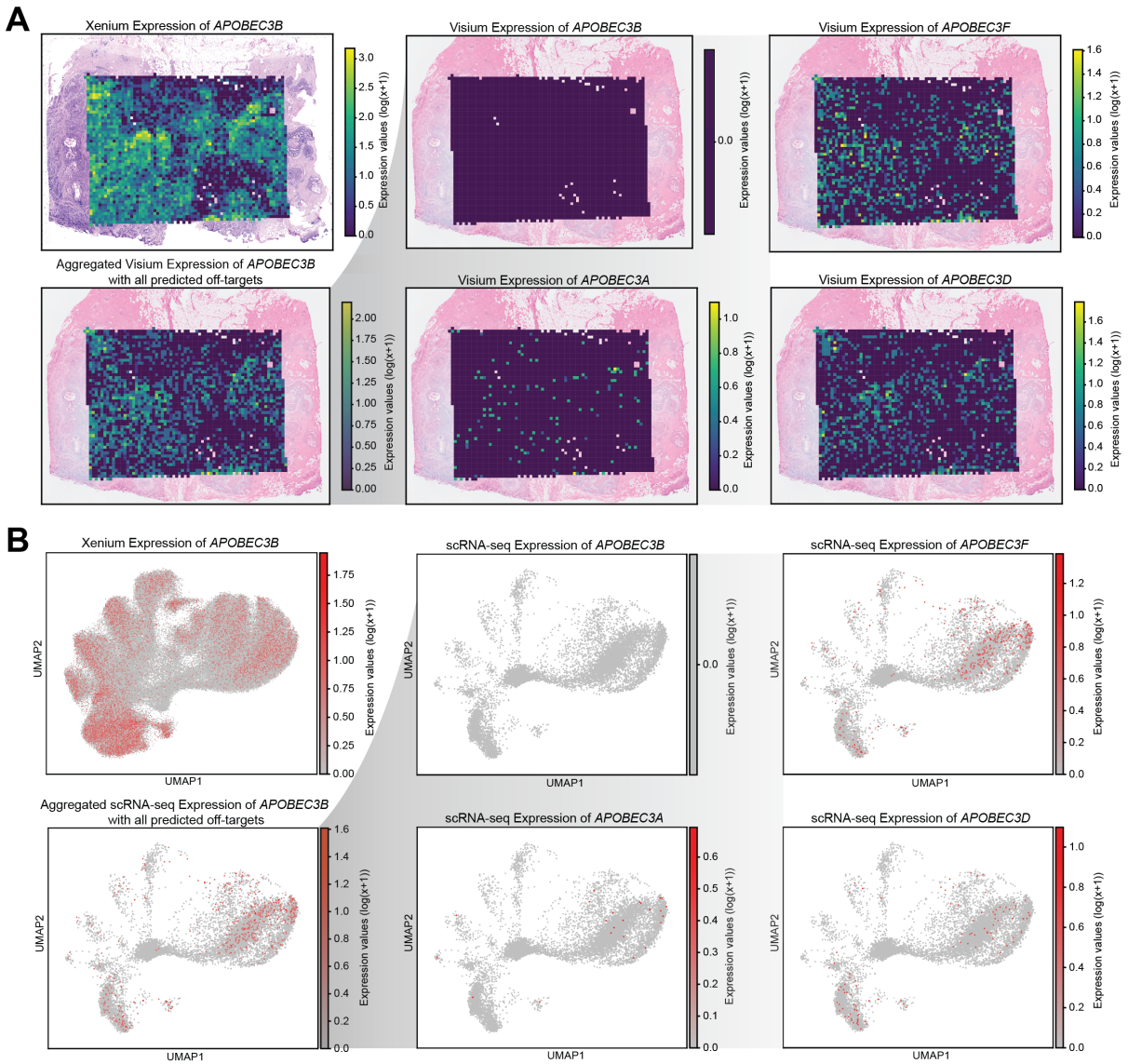

Supplementary Figure 9. (A) Spatial gene expression patterns of: *APOBEC3B* Xenium expression, *APOBEC3B* Visium expression, *APOBEC3F* Visium expression, the aggregated Visium expression combining *APOBEC3B* with all predicted off-target binding gene expression (*APOBEC3F, APOBEC3A, APOBEC3D*), *APOBEC3A* Visium expression, and *APOBEC3D* Visium expression. **(B)** Harmonized UMAP visualization of: *APOBEC3B* Xenium expression, *APOBEC3B* scRNA-seq expression, *APOBEC3F* scRNA-seq expression, the aggregated scRNA-seq expression combining *APOBEC3B* with all predicted off-target binding gene expression (*APOBEC3F, APOBEC3A, APOBEC3D*), *APOBEC3A* scRNA-seq expression, and *APOBEC3D* scRNA-seq expression.

641
642

643

644

645 **Supplementary Tables**

646

Target gene	Number of probes	Predicted binding genes	Number of probes aligned	Gene types
ADGRE5	19	ADGRE5,ADGRE2	18,1	PC,PC
ADH1B	23	ADH1B,ADH1A,ADH1C	22,3,3	PC,PC,PC
AKR1C1	21	AKR1C1,AKR1C2,AKR1C3,AKR1C4	20,1,1,1	PC,PC,PC,PC
AKR1C3	17	AKR1C3,AKR1C1,AKR1C2,AKR1C4	16,1,1,2	PC,PC,PC,PC
APOBEC3A	10	APOBEC3A,APOBEC3B	7,4	PC,PC
APOBEC3B	14	APOBEC3B,APOBEC3A, APOBEC3D,APOBEC3F	13,2,2,2	PC,PC,PC,PC
C15orf48	6	C15orf48,MIR147B	6,1	PC, precursor_RNA
CEACAM6	13	CEACAM6,CEACAM3	13,1	PC,PC
FCGR3A	20	FCGR3A,FCGR3B	20,3	PC,PC
FLNB	33	FLNB,LOC124909485	33,1	PC,PC
KLRC1	15	KLRC1,KLRC2,KLRC3, KLRC4-KLRK1,KLRC4	15,3,1,1,1	PC,PC,PC,PC,PC
KRT6B	15	KRT6B,KRT6A,KRT6C, KRT75	15,1,4,1	PC,PC,PC,PC
S100A4	5	S100A4,S100A5	3,1	PC,PC
SERHL2	8	SERHL2,SERHL	8,7	PC,misc_RNA
SLAMF1	24	SLAMF1,LOC107985220	23,1	PC,ncRNA
SVIL	20	SVIL,SVIL2P	20,2	PC,misc_RNA
TOMM7	10	TOMM7,LOC107986346	3,2	PC,PC
TPD52	21	TPD52,TPD52-MRPS28	21,5	PC,PC
TPSAB1	2	TPSAB1,TPSB2,TPSD1	2,2,1	PC,PC,PC
TUBA4A	12	TUBA4A,TUBA4B	12,1	PC,PC
TUBB2B	11	TUBB2B,TUBB2A,TUBB3, TUBB4A	11,3,1,1	PC,PC,PC,PC
ZNF562	22	ZNF562,ZNF812P	22,3	PC,misc_RNA

647
648 **Supplementary Table 1.** OPT output of genes with predicted off-target binding based on perfect
649 sequence homology in RefSeq. This table shows the 22 genes whose probes in the Xenium breast cancer
650 panel exhibit predicted off-target probe binding, where each off-target alignment involves a perfect
651 40bp match to the probe sequence. The final column shows the gene types, in order, of each of the off-
652 target genes shown in column 3. Abbreviations: PC = protein-coding; PG = pseudogene; precursor_RNA
653 = precursor RNA; misc_RNA = miscellaneous RNA; ncRNA = non-coding RNA.
654
655
656
657
658

Target gene	Number of probes	Predicted binding genes	Number of probes aligned	Gene types
ADGRE5	19	ADGRE5, ADGRE2	19,1	PC,PC
ADH1B	23	ADH1B,ADH1A,ADH1C	22,3,3	PC,PC,PC
AKR1C1	21	AKR1C1,AKR1C2,AKR1C3, AKR1C4	20,1,1,1	PC,PC,PC,PC
AKR1C3	17	AKR1C3,AKR1C1,AKR1C2, AKR1C4	17,1,1,2	PC,PC,PC,PC
APOBEC3A	14	APOBEC3B,APOBEC3A,APOBEC3D, APOBEC3F	14,2,2,2	PC,PC,PC,PC
APOBEC3B	10	APOBEC3A,APOBEC3B	8,4	PC,PC
C15orf48	6	C15orf48,MIR147B	6,1	PC,miRNA
CEACAM6	13	CEACAM6,CEACAM3	13,1	PC,PC
EPCAM	15	EPCAM,LOC132386	14,1	PC,PG
FCGR3A	20	FCGR3A,FCGR3B	20,3	PC,PC
FLNB	33	FLNB,LOC124909485	33,1	PC,PC
HMGA1	7	HMGA1,HMGA1P1,HMGA1P2, HMGA1P3,HMGA1P6	7,1,3,2,2	PC,PG,PG,PG, PG
KLRC1	15	KLRC1,KLRC2,KLRC3,KLRC4-KLRK1,KLRC4	15,3,1,1,1	PC,PC,PC,PC, PC
KRT14	6	KRT14,KRT16P6	6,1	PC,PG
KRT6B	15	KRT6B,KRT6A,KRT6C,KRT75	15,1,4,1	PC,PC,PC,PC
KRT8	18	KRT8,KRT8P36,KRT8P11,KRT8P, KRT8P2,KRT8P33,KRT8P45, KRT8P37,KRT8P30,KRT8P17, KRT8P22,KRT8P32,KRT8P42	9,1,1,3,2,2, 2,1,1,1,1,1,1	PC,PG,PG,PG, PG,PG,PG,PG, PG,PG,PG,PG, PG
LDHB	18	LDHB,LDHBP2	18,1	PC,PG
MYLK	35	MYLK,MYLKP1	29,1	PC,PG
MYO5B	20	MYO5B,MYO5BP1,MYO5BP2, LOC102724787	20,2,3,2	PC,PG,PG,PG
SCD	20	SCD,SCDP1	20,6	PC,PG
SERHL2	8	SERHL2,SERHL	8,7	PC,PG
SMS	17	SMS,LOC646347,LOC100419037, LOC642590	17,8,1,3	PC,PG,PG,PG
SVIL	20	SVIL,SVIL2P	20,2	PC,PG
TOMM7	10	TOMM7,LOC107986346	3,2	PC,PC
TPD52	21	TPD52,TPD52-MRPS28	21,5	PC,PC
TPSAB1	2	TPSAB1,TPSB2,TPSD1	2,2,1	PC,PC,PC
TRAF4	14	TRAF4,LOC100420513	14,1	PC,PG
TUBA4A	12	TUBA4A,TUBA4B	12,1	PC,PC
TUBB2B	11	TUBB2B,TUBB2A,TUBB3, TUBB4A	11,3,1,1	PC,PC,PC,PC
VOPP1	24	VOPP1,LOC729086	22,16	PC,PG

VWF	20	VWF,VWFP1	20,2	PC,PG
ZEB2	47	ZEB2,ZEB2P1	28,1	PC,PG
ZNF562	22	ZNF562,ZNF812P	22,3	PC,PG

Supplementary Table 2. OPT output of genes with predicted off-target binding based on perfect sequence homology in CHESS. This table shows the 33 genes whose probes in the Xenium breast cancer panel exhibit predicted off-target probe binding, where each off-target alignment involves a perfect 40bp match to the probe sequence. The final column shows the gene types, in order, of each of the off-target genes shown in column 3. Abbreviations: PC = protein-coding; PG = pseudogene; miRNA = microRNA.

Perfect match		**GENCODE Basic**	**GENCODE Comprehensive**	**RefSeq**	**CHESS**
Number of transcripts		158,339	387,944	181,627	158,363
All genes	Off-target probes	180	185	60	112
	Affected genes	45	45	22	33
Pseudogenes removed	Off-target probes	151	156	60	46
	Affected genes	36	36	22	17
Protein coding genes only	Off-target probes	58	58	46	45
	Affected genes	17	17	17	16

Supplementary Table 3. The number of off-target probes and affected genes (from the set of 280 genes in the Xenium panel)) found when looking for perfect matches between probe sequences and transcripts in four different reference annotations: GENCODE basic, GENCODE comprehensive, RefSeq, and CHESS. Off-target alignments between CCPG1 probes and DNAAF1-CCPG1 were excluded.

Gene	GENCODE	RefSeq	CHESS
ADGRE5	✓	✓	✓
ADH1B	✓	✓	✓
AKR1C1	✓	✓	✓
AKR1C3	✓	✓	✓
APOBEC3A	✓	✓	✓
APOBEC3B	✓	✓	✓
CEACAM6	✓	✓	✓
FCGR3A	✓	✓	✓
KLRC1	✓	✓	✓
KRT6B	✓	✓	✓
TPSAB1	✓	✓	✓
TUBA4A	✓	✓	✓
TUBB2B	✓	✓	✓
AQP1	✓	x	x
C1QA	✓	x	x
CD79B	✓	x	x
FLNB	x	✓	✓
PDGFRA	✓	x	x
S100A4	x	✓	x
TOMM7	x	✓	✓
TPD52	x	✓	✓

Supplementary Table 4. Union set of protein coding genes that OPT predicts to be affected by off-target binding, across three different reference annotations: GENCODE basic and comprehensive, RefSeq, and CHESS. Genes not shared across all four annotations are colored in red.

Target gene	Number of probes	Binding genes	Number of probes aligned	Gene types – GENCODE (v47)
ACTG2	18	ACTBP2,ACTG1P11,ACTG1P2	1,2,2	PG,PG,PG
ANKRD30A	20	ENSG00000215398, ENSG00000215512, ENSG00000290354	1,1,1	PG,PG,lncRNA
APOC1	2	APOC1P1	1	lncRNA
CD83	20	CD83P1	1	PG
CEACAM8	13	CEACAM5,CEACAM6,CEACAM7, CEACAMP8,PSG6	1,1,1,1,1	PC,PC,PC,PG,PC
CXCL5	16	CXCL6	1	PC
ENAH	20	ENAHP1	2	PG
FLNB	33	ENSG00000263343	1	PG
KRT5	13	KRT6B,KRT75	1,1	PC,PC

Supplementary Table 5. Nine additional genes that were identified to exhibit potential off-target probe binding when allowing for a 6bp error margin on either side of the binding site. Abbreviations: PC = protein-coding; PG = pseudogene; lncRNA = long non-coding RNA.

Target gene	Number of probes	Additional binding genes	Number of additional probes aligned	Gene types – GENCODE (v47)
ADH1B	22	ADH1A,ADH1C	1,2	PC,PC
AKR1C1	21	AKR1C3,AKR1C2	1,1	PC,PC
AKR1C3	17	AKR1C2,AKR1C1,AKR1C5P	1,2,1	PC,PC,PG
APOBEC3A	8	APOBEC3D	1	PC
CEACAM6	13	CEACAM5,CEACAM7,CEACAM8	1,1,1	PC,PC,PC
FCGR3A	20	FCGR3B,ENSG00000289768	8,1	PC,PC
KRT14	6	ENSG00000290977,KRT16P6, ENSG00000290978,KRT16,KRT16P2	1,1,1,1,1	lncRNA,PG, lncRNA,PC,PG
KRT6B	15	KRT6A,KRT5	2,1	PC,PC
KRT8	18	KRT8P32,KRT8P36, ENSG00000235286,GFAP,KRT8P14, KRT8P15,KRT8P31,KRT8P35, KRT8P43,KRT8P46,KRT8P47, KRT8P48,KRT8P49,KRT8P7,KRT8P9	1,1,1,1,1, 1,2,1,1,1, 1,1,1,1,1	PG,PG,PG,PC, PG,PG,PG,PG, PG,PG,PG,PG, PG,PG,PG
LDHB	18	LDHBP1	1	PG
LILRA4	16	ENSG00000299952,LILRA6,LILRB3, LILRP1,LILRP2	1,2,2,1,2	lncRNA,PC,PC, PG,lncRNA
MYO5B	20	MYO5BP3	1	PG
PTGDS	5	ENSG00000284341	1	NMD
SMS	17	ENSG00000213080, ENSG00000232389, ENSG00000251342	2,4,1	PG,PG,PG
SVIL	20	ENSG00000290952, ENSG00000304099	1,1	lncRNA, lncRNA
TUBB2B	11	ENSG00000198211,TUBB3,TUBB4A, TUBB4B,TUBB4BP3	1,1,1,1,1	PC,PC,PC,PC,PG
VWF	20	VWFP1	1	PG
ZNF562	22	ENSG00000291231,ZNF812P, ENSG00000226810,ENSG00000267490, ZNF561	1,1,1,1,1	lncRNA,PG, PG,PG,PC

Supplementary Table 6. Eighteen genes that were previously predicted to be affected by off-target binding based on perfect matching now show additional predicted off-target interactions when a 6bp error margin is allowed on either side of the binding site. This effect is observed either through the accumulation of new probes with predicted off-target binding or via the identification of additional predicted off-target genes per probe. Abbreviations: PC = protein-coding; PG = pseudogene; lncRNA = long non-coding RNA.

736 **Supplementary Data**

737 To access a copy of the Xenium v1 Breast Gene Expression Panel fasta file, open the attached
738 Supplementary Data zip file
739 'xenium_human_breast_gene_expression_panel_probe_sequences.fasta.zip'